Tumor Cell Uptake and Selectivity of Gadolinium(III)-Phosphonium Complexes: The Role of Delocalisation at the Phosphonium Centre

*Madleen Busse,[a] Madeline S. A. Windsor,[a] Alexander Tefay,[a] Elaine Kardashinsky,[a] Jacob M. Fenton,[a] Daniel E. Morrison,[a] Hugh H. Harris,[b] and Louis M. Rendina[a]**

[a] *School of Chemistry, The University of Sydney, Sydney, NSW 2006, Australia.*

Tel: +61 2 9351 4781; Fax: +61 2 9351 3329; lou.rendina@sydney.edu.au

[b] *Department of Chemistry, The University of Adelaide, Adelaide, SA 5005, Australia.*

Graphical Abstract

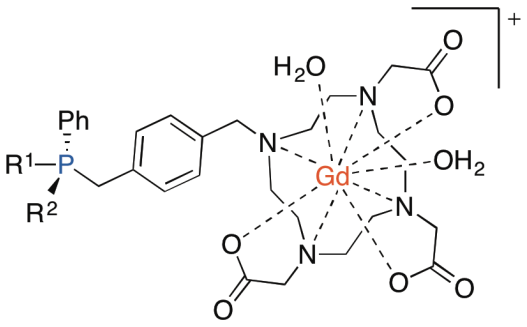

1: $R^1 = R^2 = Ph$
2: $R^1 = Ph$, $R^2 = Me$
3: $R^1 = R^2 = Me$

The synthesis of bifunctional Gd(III)-phosphonium complexes possessing a varying degree of delocalisation at the phosphonium centre is reported. Cellular uptake studies indicate that a reduced delocalisation at the phosphonium centre can lead to greater Gd uptake into normal cells, resulting in a decrease in the overall tumor cell selectivity.

Highlights

- A series of bifunctional Gd(III)-phosphonium complexes were synthesised.
- The Gd complexes possess a varying degree of delocalisation at the phosphonium centre.
- A reduced delocalisation at the phosphonium centre led to decreased tumor cell selectivity.
- Synchrotron X-ray fluorescence (XRF) imaging of a population of glioma cells is reported.
- The XRF maps show dispersed spots of high intensity due to mitochondrial uptake of Gd.

Keywords

Gadolinium, phosphonium, glioblastoma, mitochondria, XRF spectroscopy

Abstract

The synthesis of a series of bifunctional Gd(III) complexes **1 – 3** covalently bound to arylphosphonium cations possessing a varying degree of delocalisation at the phosphonium centre is presented. The influence of the degree of delocalisation was investigated with regards to *in vitro* cytotoxicity, cellular uptake of Gd, tumor-cell selectivity and intracellular localisation of Gd within human glioblastoma (T98G) and human glial (SVG p12) cells. Cellular uptake and selectivity studies for the Gd(III) complexes indicate that a reduced delocalisation at the phosphonium centre can lead to greater Gd uptake into SVG p12 cells which results in a decrease in the overall tumor cell selectivity. Synchrotron X-ray fluorescence (microbeam XRF) imaging has demonstrated for the first time that uniform uptake of Gd(III) complex **2** within a population of T98G cells increased as a function of increasing Gd incubation times. The Gd maps show dispersed spots of high intensity which are consistent with mitochondrial uptake.

Introduction

The application of Gd(III) complexes in medicine today is exclusively focused upon diagnostics, and is exemplified by the use of Gd(III) complexes as water relaxation agents to improve image contrast in magnetic resonance imaging (MRI) [1-3]. More recently, an emphasis has been placed on the design of Gd(III) agents for therapeutic applications [4-6]. In particular, binary therapies for the treatment of aggressive and intractable cancers such as those of the malignant brain tumor known as glioblastoma multiforme (GBM) are of great interest [7]. Binary cancer therapies seek to address those limitations present in traditional cancer therapies, such as collateral damage to a patient's healthy tissue, by using two relatively non-toxic components which upon combination initiate a powerful cytotoxic effect *in situ*. In doing so, the treatment gains a greater level of control and selectivity. Of particular interest are the experimental binary therapies known as neutron capture therapy (NCT) [8-12] and photon activation therapy (PAT) [13-15] which utilize a non-tumor selective component such as neutrons or high-energy X-ray photons and a tumor-selective agent with low cytotoxicity. The unique nuclear and high-*Z* properties of Gd allow for the implementation of 'theranostic' Gd(III) complexes for potential use in NCT (when the naturally-occurring ^{157}Gd and ^{155}Gd isotopes are used) and PAT, respectively. In addition, due to its highly paramagnetic nature, the lanthanoid ion can also be used in MRI imaging. However, clinically-suitable Gd theranostics for application in binary cancer therapies have yet to be developed [7-15].

The therapeutically-relevant decay products in NCT and PAT appear to be Auger and Coster-Krönig (ACK) electrons, which possess an extremely short path-length (< 12 nm) [16]. Thus, the development of tumor-selective agents which can accumulate

within critical sub-cellular components such as DNA and mitochondria are an essential requirement when considering the design of new Gd agents for binary therapies [7,10,17-19]. Extensive damage to either of these important biological entities can lead to apoptosis [7,20-22].

Tumor cells typically possess an elevated mitochondrial membrane potential compared to that of normal, healthy cells (*ca.* 60 mV), which enables delocalised lipophilic cations (DLCs) such as phosphonium salts to accumulate in mitochondria with high selectivity [23-25]. In particular, tetraphenylphosphonium (TPP) and triphenylmethylphosphonium (TPMP) cations have demonstrated highly selective uptake in brain tumors *in vivo*, with a tumor to normal (T/N) tissue ratio of 40:1 and 48:1, respectively [26,27]. Based on these results, we investigated the influence of delocalisation at the phosphonium centre for a series of Gd(III)-phosphonium salts **1 – 3** with regards to *in vitro* cytotoxicity, cellular uptake, selectivity studies and intracellular Gd localization.

Results and Discussion

Syntheses

From the outset, a robust macrocyclic ligand was selected to complex Gd(III) for mitochondrial targeting. Clinical MRI agents based upon acyclic systems such as diethylenetriaminepentaacetic acid (DTPA), e.g. Magnevist®, have not shown detectable decomposition, accumulation or serum protein binding and are rapidly excreted from the body [28]. However, the US Federal Drug Administration (FDA) and the Danish Medicines Agency (DMA) have raised scrutiny with regards to kidney toxicity for such agents. Numerous cases of nephrogenic systemic fibrosis or nephrogenic fibrosing dermopathy have arisen in patients with pre-existing renal dysfunction who have been treated with the acyclic chelated Gd(III) agents including Magnevist® and Omniscan® [29]. In contrast, MRI agents such as Gd-DOTA (DOTA = 1,4,7,10-tetraazacyclododecane-1,4,7,10-tetraacetic acid) appear to be clinically safe, and thus the macrocyclic ligands used in this work were closely related to this particular entity. The new Gd(III) complexes **2** and **3** were prepared by means of a three-step synthetic procedure (Scheme 1), which was previously used in the synthesis of the archetypal Gd(III)-triphenylphosphonium complex **1** [17]. Briefly, arylphosphines were reacted with *para*-dibromoxylene in toluene to form exclusively the mono-substituted phosphonium salt intermediates. Subsequent *N*-alkylation of the tri-*tert*-butyl ester of 1,4,7,10-tetraazacyclododecane-1,4,7-triacetic acid hydrobromide (DO3A-^{t}Bu$_3$·HBr), followed by acid deprotection of the ^{t}Bu groups with TFA in CH_2Cl_2, afforded the free macrocyclic ligands in good yield and purity after purification by means of reverse-phase HPLC. The final step of the synthesis involved the treatment of the free macrocyclic ligands with a suspension of Gd_2O_3 in

H_2O to give the target Gd(III) complexes **2** and **3** in high yields (> 85%). The identities of complexes **2** and **3** were confirmed by means of high resolution ESI-FTICR-MS (**2**: $[M\text{-}CF_3CO_2]^+$: calculated *m/z* 804.21635; found 804.21613; **3:** $[M\text{-}CF_3CO_2]^+$: calculated *m/z* 742.20045; found 742.20064) and their purity (>95%) was confirmed by means of analytical reverse-phase HPLC. A series of qualitative experiments in aqueous media at biologically significant pH (7.4) and more acidic conditions (pH 5.0) followed by incubation at 37 °C for prolonged periods demonstrated excellent aqueous stability for all complexes. ESI-MS confirmed the robustness of the complexes, even after 24 h in aqueous solution.

[Scheme 1 inserted here]

Cytotoxicity Studies

In vitro cytotoxicity is reported as the half-maximal inhibitory concentration, IC_{50}, i.e. the concentration of Gd(III) complex required to inhibit 50% of cell growth. For the purposes of this study, the key point of the Gd agent is not to be acutely cytotoxic since the actual cytotoxic event in NCT or PAT involves thermal neutron or X-ray photon capture by the $^{157/155}$Gd nuclei or Gd(III) ion, respectively. Minimal cytotoxicity of this drug will ensure that if the drug enters healthy tissue there is a low likelihood of cell death resulting from the Gd agent alone.

Standard MTT assays [30] were performed on each of the Gd(III) complexes in order to assess the *in vitro* cytotoxicity against the human glioblastoma cell line (T98G). Since the IC_{50} value for complex **1** has previously been determined to be 2.55 ± 0.33 mM [17], the MTT assays for complexes **2** and **3** were performed over a 0 – 4 mM concentration range. The IC_{50} values for both these complexes were also found to be

in the low mM range (**Table 1**), which agrees with previously reported trends for cytotoxicity pertaining to this class of Gd agents [17,18].

[Table 1 inserted here]

Complexes **1 – 3** were also found to be low in cytotoxicity in comparison to the therapeutic agent Motexafin-Gadolinium (MGd), the archetypal GdNCT/GdPAT agent [4-6,14,15] whereby a concentration as low as 50 μM of MGd results in tumor suppression in the absence of X-ray irradiation [31]. Furthermore, the concentrations reported in a study of MGd by De Stasio *et al*. [7] are well below the IC_{50} values determined for complexes **1 – 3**. Notably, the phosphonium salt TPMP has an IC_{50} value of 123 μM [32] which again highlights the low *in vitro* cytotoxicities of complexes **1 – 3**.

Cell Uptake Studies

Complexes **1 – 3** were analysed for their uptake into the T98G human glioblastoma cell line and the non-cancerous SVG p12 human fetal glial cell line by means of ICP-MS. The high sensitivity of ICP-MS makes it a very useful method to analyse low metal content in biological samples. Gd(III) levels in biological samples have previously been analysed using this method [7,17,18,20].

Each Gd(III) complex was dosed at three concentrations (10 μM, 100 μM and 1000 μM), all of which were below their IC_{50} values (*vide supra*). Protein content was determined by the BCA protein assay [33] and cell counts were determined using a Countess® Automated Cell Counter (Life Technologies). The cellular Gd content was normalised to the protein content and cell count such that Gd uptake is expressed as ng Gd/mg protein and also as the total number of Gd atoms per cell. The three

complexes **1 – 3** assessed for *in vitro* cellular uptake showed very high uptake in both cell lines when compared to the controls (Table 2). The exact mechanism for the cellular uptake of these complexes is currently unknown but these results clearly indicate that the Gd(III) complexes are able to traverse the cell membrane and enter the intracellular space. Previous work with **1** confirms cellular uptake and mitochondrial aggregation by the complex, and presumably the related complexes **2** and **3** follow a similar fate. Furthermore, the simpler Gd-DOTA (DOTA = 1,4,7,10-tetraazacyclododecance-1,4,7,10-tetraacetic acid) complex is an extracellular, water-soluble contrast agent used in MRI [34], and it does not readily enter cells. Hence, the ability of complex **1** to enter the intracellular space and localise in mitochondria can in largely be attributed to the phosphonium centre.

[Table 2 inserted here]

The results obtained from the cell uptake studies were statistically analysed by means of an ordinary two-way ANOVA followed by Sidak's multiple comparison tests (Figure 1). The analyses resulted in a statistically significant Gd uptake, i.e. the effect of the treatment (control or complexes **1 – 3**) differs between the T98G and SVG p12 cell lines.

[Figure 1 inserted here]

Here, the overall trend showed that the uptake of complex **2** is significantly greater in T98G cells compared to SVG p12 cells. At low concentrations (10 μM), treatment with either complex **1** or **2** resulted in significantly higher uptake into T98G cells compared to SVG p12 cells. For the control and complex **3**, however, a statistically significant difference in uptake between the two cell lines was not observed.

Alternatively, one can examine the effect of the Gd treatment (i.e. difference between control and complexes **1 – 3**) on either T98G or SVG p12 cells (Figure 2). The interpretation of the overall statistical significance was again focused on the Sidak's multiple comparison post tests, e.g. is Gd uptake statistically significant for complex **2**? This analysis yielded an overall trend for complex **2** showing significant greater uptake in T98G cells compared to complexes **1** and **3** at all concentrations (10 μM, 100 μM, and 1000 μM). In contrast, no statistically significant difference in cell uptake for complexes **1 – 3** was found in SVGp12 cells.

[Figure 2 inserted here]

Differences in cell uptake and aggregation of complexes **1 – 3** must be the result of the structural differences associated with the phosphonium group. An apparent decrease in delocalisation at the phosphonium centre by replacement of one Ph group in **1** with a Me group (complex **2**) leads to significantly greater uptake into T98G cells for complex **2**, compared to that observed for complex **1**. However, a further reduction of delocalisation at the phosphonium centre in complex **3** by the use of a single phenyl group and two methyl groups does not further enhance cell uptake in T98G cells. Steric and lipophilic effects might also play some role in these observed differences in cell uptake. However, the difference in log*P* values between **1** and **2** is only 0.03 ± 0.01 units (as determined by HPLC), thus indicating that differences in lipophilicity play only a marginal role, if any, in the cell uptake of these complexes. Furthermore, the replacement of one phenyl group by a similarly-sized cyclohexyl group in **1** results in a Gd(III) complex exhibiting comparable cellular uptake characteristics to complex **2** (unpublished data), and thus steric differences are also unlikely to play a significant role in determining cellular uptake. Organic

cation transporters (OCTs) of the SLC22 gene family are currently being investigated as another potential point of difference and will be reported in due course.

Tumor Cell Selectivity Studies

The ratio of tumor cell to normal cell uptake (T/N) provides an indication of the *in vitro* selectivity of the complexes **1 – 3**. The *in vitro* T/N selectivity for tumor cells was calculated by determining the ratio of Gd uptake into the tumor cell line T98G *vs.* the normal cell line SVG p12 (Table 2). The results showed that a decrease in the T/N selectivity occurred with increasing Gd concentrations, i.e. a concentration of 10 μM yielded the highest T/N ratio. Interestingly, *in vitro* selectivity is completely lost at the highest concentration used in these experiments (1000 μM), which might indicate a change in the uptake mechanism of the complexes **1 – 3** at high concentrations. The results obtained from the selectivity studies were statistically analysed by means of an ordinary two-way ANOVA followed by Sidak's multiple comparison post tests (Figure 3). The analysis resulted in a statistically significant outcome, i.e. the effect of the three concentrations (10 μM, 100 μM, and 1000 μM) differs between the control and complexes **1 – 3**.

[Figure 3 inserted here]

The *in vitro* selectivity of complex **1** (13.2 ± 2.1) at a concentration of 10 μM is significantly greater compared to complexes **2** and **3**. At higher Gd concentrations, no significance in T/N selectivity was observed between complexes **1 – 3**. This result indicates that alkyl/aryl modifications at the phosphonium centre do not lead to a significantly greater T/N ratio, even though the *overall* uptake into T98G cells was

observed to be significantly greater when a methyl group replaces phenyl at the phosphonium centre.

Synchrotron X-ray Fluorescence (XRF) Studies

Synchrotron X-ray fluorescence (XRF) studies were performed on T98G cells treated with the complexes **1** and **2** to allow for the visualisation of elemental distribution within cells. Complex **1** has been extensively investigated on individual cells providing strong evidence of mitochondrial accumulation within such cells [17]. Since the Gd localisation within a *single cell* had been previously determined for this class of complexes, the aim of this study was to overcome the inherent statistical limitations of single cell imaging. Studies were carried out by imaging all T98G cells grown on Si_3N_4 windows (1.5 x 1.5 mm), which were fixed with 1% paraformaldehyde solution. Data were collected for control cells and cells treated with 100 μM of complex **2** for 6 h and 24 h. Figure 4 shows a magnified view (representative area covering *ca.* 20% of the total scan area) of inelastic scatter (Compton) maps of incident photons, which were a useful guide to identify cell boundaries. The elemental maps for Zn are in very good agreement with the Compton maps. Zn was selected as it is an essential element present in cells with endogenous Zn levels occurring within the experimental detection limits [35], and, therefore, the element is a useful guide to clearly identify cell boundaries of individual cells or cell aggregates. The XRF quantification of intracellular Zn content was found to be constant across both cell lines and independent of the treatment with complex **2**. The detected average elemental area density of 0.0060 ± 0.0014 μg cm^{-2} is in good agreement with the endogenous Zn content previously reported for T98G cells [17]. As expected, Gd concentrations associated with untreated T98G cells were below the

experimental detection limits and are consistent with the low abundance of Gd in biological systems, i.e. the observed Gd levels found in treated T98G cells are attributed entirely to complex **2**. The Gd maps show dispersed spots of high intensity at both 6 h and 24 h post-treatment which are consistent with mitochondrial uptake, as demonstrated previously for related Gd(III) complexes [17,18]. The elemental density maps of those cells dosed with **2** also showed a negative correlation of the Gd regions to areas of high intensity in the Zn maps; regions of high Zn density are indicative of the cell nucleus due to the presence of Zn finger proteins. The XRF quantification of intracellular Gd yielded elemental area densities of 0.63 ± 0.05 μg cm^{-2} after 6 h and 0.82 ± 0.06 μg cm^{-2} after 24 h of treatment showing an increase of Gd within cells with increasing incubation times. The observed levels of Gd were found to be constant over the total scan area suggesting that within one T98G cell population the uptake of complex **2** is uniform.

[Figure 4 inserted here]

In order to distinguish cells from non-cellular debris, a mask of each cell position was constructed (Figure 5). These masks were derived from the inelastic scatter and high resolution Zn maps using *ImageJ* (v1.49j). The quality of the mask was assessed by co-registering the binary image with the elemental maps of Zn and Gd. A good agreement is seen for the overlay of the mask with the elemental maps confirming once again the accumulation of Gd occurs in all scanned T98G cells.

[Figure 5 inserted here]

Conclusion

The new Gd(III) complexes **2** and **3** were successfully synthesised in high yields and purity. The complexes were found to be low in cytotoxicity at therapeutically-relevant concentrations. The observed cell uptake and selectivity results for complexes **1 – 3** indicate that differences in lipophilicity and steric bulk at the phosphonium centre do not appear to be correlated to their significant uptake into tumor cells, whilst reduced delocalisation around the phosphonium centre appears to result in greater uptake into normal cells causing a decrease in overall *in vitro* selectivity. For example, complex **2** showed significantly greater uptake into the T98G cell line compared to complex **1**, whilst its overall T/N selectivity was diminished due to its increased accumulation in the normal cell line SVG p12.

These results also indicate that more than one cell uptake mechanism may be involved. One mechanism appears to act at lower Gd(III) complex concentrations whilst a different uptake mechanism takes over once the concentration of the complexes exceeds a certain limit. Lower concentrations of Gd(III) complex are more selective for tumor cells and deliver a significant number of Gd atoms to each of the cells. In summary, the new complexes **1 – 3** exhibit comparable accumulation and selectivity for T98G cells as MGd, which has been previously explored clinically as a radiation sensitizer [7,36].

The accumulation of complex **2** in T98G cells was further confirmed by synchrotron XRF studies showing an expected increase of intracellular Gd content with respect to the exposure times of 6 h and 24 h. This study allowed for the XRF quantification of intracellular Gd content for a large number of cells, thus overcoming the statistical

limitations inherent in single cell XRF imaging. In the case of the scanned T98G cells, a constant Gd level was observed suggesting a uniform accumulation of the drug within one T98G population. The Gd maps show dispersed spots of high intensity which are consistent with mitochondrial uptake [17,18]. Furthermore, the elemental density maps of those cells dosed with **2** also showed a negative correlation of the Gd regions to regions of high intensity in the Zn maps.

Materials and Methods

All precursors were purchased from Sigma-Aldrich, except where otherwise stated. Distilled water was used for all experiments requiring water. Toluene was dried over sodium wire and freshly distilled prior to use, according to the procedure by Armarego and Chai [37]. Et_2O was dried over sodium wire and freshly distilled. All other solvents were used without further purification. Reactions requiring inert atmospheres were performed under a dry nitrogen atmosphere using conventional Schlenk techniques [38]. Dimethylphenylphosphine was handled in a glove bag.

All ^{1}H, $^{1}H\{^{31}P\}$, $^{13}C\{^{1}H\}$, and $^{31}P\{^{1}H\}$ NMR spectra were recorded at 300 K on a Bruker Avance300 spectrometer (^{1}H at 300 MHz, ^{13}C at 75 MHz, ^{31}P at 121 MHz). All NMR signals (δ) are reported in ppm. ^{1}H, $^{1}H\{^{31}P\}$ and $^{13}C\{^{1}H\}$ NMR spectra were referenced according to their solvent residual peaks. $^{31}P\{^{1}H\}$ NMR spectra were referenced to external $P(OMe)_3$ at 140.85 ppm. IR spectra were recorded on a Bruker FT-IR Tensor 27 using KBr. Melting points were recorded on an MPA161 Digital Melting Point Apparatus. Low resolution ESI-MS were recorded on a Finnigan LCQ mass spectrometer. High resolution ESI-FTICR-MS data was recorded on a Bruker 7.0T mass spectrometer. Preparative HPLC was performed on a Waters 600 HPLC system with a Waters 486 tuneable absorbance UV/vis detector (λ = 254 nm) and a Sunfire C18 preparative column (19 × 150 mm, 5 μm pore size). Flow rate 7 mL/min. HPLC was performed under gradient flow conditions, starting with 100% Solvent A (Milli-Q water with 0.1% trifluoroacetic acid) and 0% Solvent B (liquid chromatography-grade acetonitrile with 0.1% trifluoroacetic acid) and moving to 0% Solvent A and 100% Solvent B over 45 min. Analytical HPLC was performed on a Waters 2965 separation module HPLC system with a Waters 2996 photodiode array

(PDA) detector (λ = 300 to 200 nm) and a Sunfire C18 analytical column (2.1 × 150 mm, 5 μm pore size). Flow rate 0.2 mL/min. HPLC was performed under gradient flow conditions, starting with 100% Solvent A (Milli-Q water with 0.1% trifluoroacetic acid) and 0% Solvent B (Liquid chromatography-grade acetonitrile with 0.1% trifluoroacetic acid) and moving to 0% Solvent A and 100% Solvent B over 45 min.

Synthetic methods

General ligand procedure GP1: A phosphine of the general formula $PR^1R^2R^3$ (R^1 = R^2 = Ph, R^3 = Me; R^1 = R^2 = Me, R^3 = Ph) was dissolved in toluene (20 mL) and added dropwise to a solution of *α,α'*-dibromomethyl-*p*-xylene in the same solvent (20 mL). The reaction mixture was stirred at reflux for 4 h. The desired *mono*-substituted phosphonium bromide which crystallised from the reaction mixture was filtered off, washed with toluene (30 mL) and dried *in vacuo* to yield a colorless solid.

General ligand procedure GP2: The phosphonium bromide prepared above (1 eq) was stirred at reflux with DO3A-^{t}Bu$_3$·HBr (1.7 g, 2.8 mmol; 1 eq) and Na_2CO_3 (0.29 g, 3 mmol; 1 eq) in acetonitrile (20 mL) for 16 h. The white precipitate was filtered off and the filtrate was reduced *in vacuo* to afford clear yellow oil. The *tert*-butyl protected ligand was dissolved in 20 mL of a 50% trifluoroacetic acid/CH_2Cl_2 mixture and stirred at room temperature for 16 h. The solvent was removed *in vacuo* and the crude residue was extracted with $CHCl_3$ (3 x 50 mL). The aqueous layer was reduced *in vacuo* to yield an off-white solid which was purified by reverse-phase HPLC and lyophilised to afford the free ligand as a white powder.

General complexation procedure GP3: The free bifunctional ligand prepared above was stirred as a suspension with an excess of Gd_2O_3 (2 eq) in H_2O at 80^{o}C for

12 h. Unreacted and insoluble Gd_2O_3 was removed by means of centrifugation. The filtrate was reduced *in vacuo* and the product lyophilised to afford the Gd(III) complex as a white powder. The purity of the Gd(III) complex was confirmed by means of reverse-phase HPLC.

4,7,10-tris(2-(*tert*-butoxy)-2-oxoethyl)-4,7,10-triazaazoniacyclododecane-1-ium bromide (DO3A-^{t}Bu$_3$·HBr): This procedure was adapted from the one reported by Moore [39]. A solution of 1,4,7,10-tetraazacyclododecane (cyclen) (13.5 g, 78.5 mmol) and NaOAc (34.8 g, 424 mmol) in dimethylacetamide (DMA) (110 mL) was stirred for 30 min in an ice-MeOH bath. A solution of *tert*-butylbromoacetate (37.5 mL) and DMA (55 mL) was added dropwise to the stirred solution over 60 min. The resulting solution was allowed to equilibrate to RT and was stirred for 65 h. The mixture was diluted with Et_2O (50 mL), placed in an ice-MeOH bath and stirred for a further 2 h. A white precipitate formed and it was filtered off and washed with cold DMA (30 mL) and then cold Et_2O (130 mL) to afford a white powder. The white powder was dissolved in $CHCl_3$ (250 mL), washed with water (2 × 40 mL), and saturated NaBr solution (40 mL). The organic layer was dried over $MgSO_4$ and the filtrate reduced *in vacuo* to an oil (~100 mL). Crystallisation was afforded by the addition of *n*-hexane to the oil and stirring the mixture at RT for 3 h then a further 2 h of stirring in an ice-MeOH bath. The white precipitate was collected by filtration and washed with cold *n*-hexane/$CHCl_3$ (4:1, 70 mL) and dried *in vacuo*. Yield 26.4 g (57.4%). ^{1}H NMR ($CDCl_3$): δ = 10.04 (br s, 2H, N***H***$_2$), 3.38 (s, 4H, C***H***$_2$), 3.30 (s, 2H, C***H***$_2$), 3.11 (m, 4H, C***H***$_2$), 2.92 (m, 8H, C***H***$_2$), 2.89 (m, 4H, C***H***$_2$), 1.44 (s, 27H, C***H***$_3$). ^{13}C{^{1}H} NMR ($CDCl_3$): δ = 170.9 (C=O), 170.0 (C=O), 82.3 (C_q), 82.1 (C_q), 58.6 (CH_2), 51.8 (CH_2), 51.7 (CH_2), 49.6 (CH_2), 49.3 (CH_2), 47.9 (s, CH_2), 28.6 (s, CH_3).

Complex 1: The Gd(III) complex **1** was synthesized and characterized as reported previously.[7a] Complex **1** was HPLC purified (T_R = 16.5 min) and its identity confirmed by means of ESI-FTICR-MS for $[M - CF_3CO_2]^+$: Calculated *m/z* 866.23211; Found 866.22992.

Complex 2: A solution of methyldiphenylphosphine (0.52 mL, ρ = 0.97 g cm^{-3}, 0.50 g, 2.52 mmol) in dry toluene was added dropwise to a solution of *α,α'*-dibromomethyl-*p*-xylene (1.00 g, 3.79 mmol) in dry toluene. The desired phosphonium bromide was obtained according to **GP1**. Yield 0.82 g (70%). $^1H\{^{31}P\}$ NMR ($CDCl_3$): δ = 7.97-7.87 (m, 4H, P-*o*-Ph***H***), 7.70-7.60 (m, 6H, P-*p*-Ph***H*** and P-*m*-Ph***H***), 7.32-7.11 (m, 4H, benzyl linker Ph***H***), 5.02-4.94 (d, 2H, PC***H₂***, $^2J_{HP}$ = 15.2 Hz), 4.38 (s, 2H, BrC***H***$_2$), 2.72 (d, 2H, PC***H***$_3$, $^2J_{HP}$ = 13.6 Hz). $^{13}C\{^1H\}$ NMR ($CDCl_3$): δ = 137.9 ($BrCH_2$***C***), 134.7 (P-*p*-Ph***C***), 133.1 (P-*o*-Ph***C***), 131.4 (PCH_2C***C***H), 130.1 (P-*m*Ph***C***), 129.5 ($BrCH_2C$***C***H), 128.0 (PCh_2***C***), 118.7 (P***C***), 32.9 (Br***C***H_2), 30.7 (P***C***H_2), 7.3 (P***C***H_3). $^{31}P\{^1H\}$ NMR ($CDCl_3$): 23.0. ESI-MS (MeOH): *m/z* = 382.80 ($[M - Br]^+$). The synthesis was continued according to **GP2** whereby 0.20 g (0.43 mmol) of freshly-synthesized phosphonium bromide was used. HPLC fractions were collected at 16.6 min to afford the desired deprotected bifunctional ligand. Yield 0.13 g (40%). T_R = 16.6 min. $^1H\{^{31}P\}$ NMR (D_2O): δ = 7.80-7.59 (m, 10H, P-Ph***H***), 7.42 (d, 2H, $^3J_{HH}$ = 7.78, PCH_2CC***H***), 7.08 (d, 2H, $^3J_{HH}$ = 7.85 Hz, NCH_2CC***H***), 4.35 (s, 2H, PC***H***$_2$), 4.07-3.09 (br m, 24H, C***H***$_2$), 2.74 (s, 3H, PC***H***$_3$). $^{13}C\{^1H\}$ NMR (D_2O): δ = 135.1 (***C***$_{aryl}$), 132.4 (***C***$_{aryl}$), 131.6 (***C***$_{aryl}$), 130.0 (***C***$_{aryl}$), 118.6 (***C***$_{aryl}$), 57.4 (***C***H_2), 54.7 (***C***H_2), 53.0 (***C***H_2), 51.4 (***C***H_2), 49.7 (***C***H_2), 48.3 (***C***H_2), 29.8 (***C***H_2), 5.4 (***C***H_3). $^{31}P\{^1H\}$ NMR (D_2O): δ = 21.9. ^{19}F (D_2O): δ = -75.87. ESI-FT-ICR-MS for $[M - CF_3CO_2]^+$: Calculated *m/z* 649.31495; Found 649.31490. Gd(III) complex **2** was synthesized according to **GP3**

using 0.100 g (0.13 mmol) of freshly-synthesized and deprotected bifunctional ligand. HPLC fractions were collected at 16.4 min to afford the desired product. Yield 0.11 g (92%). T_R = 16.4 min. IR (KBr, cm^{-1}): $\tilde{\nu}$ = 1681 (C=O), TFA^-), 1594 (C=O), DO3A). M.p.>260°C (dec.). ESI-FTICR-MS for $[M - CF_3CO_2]^+$: Calculated *m/z* 804.21635; Found 804.21613.

Complex 3: A solution of dimethylphenylphosphine (1 mL, ρ = 0.97 g cm^{-3}, 0.97 g, 7.02 mmol) in dry toluene was added dropwise to a solution of *α,α'*-dibromomethyl-*p*-xylene (2.10 g, 8.0 mmol) in dry toluene cooled in an ice bath. The reaction mixture was then stirred at RT until a precipitate formed. The resulting phosphonium bromide was isolated according to **GP1**. Yield 2.2 g (77%). $^1H\{^{31}P\}$ NMR (CD_3OD): δ = 7.93-7.90 (m, 2H, P-*o*-Ph***H***), 7.84-7.79 (m, 1H, P-*p*-Ph***H***), 7.72-7.67 (m, 2H, P-*m*-Ph***H***), 7.39-7.14 (m, 4H, benzyl linker Ph***H***), 4.56 (s, 2H, BrC***H***$_2$), 4.20 (s, 2H, PC***H***$_2$), 2.32 (s, 6H, PC***H***$_3$). $^{13}C\{^1H\}$ NMR (CD_3OD): δ = 140.1 ($BrCH_2$***C***), 135.8 (P-*p*-Ph***C***), 133.2 (P-*o*-Ph***C***), 131.8 (PCH_2C***C***H), 131.1 (P-*m*-Ph***C***), 130.0 ($BrCH_2C$***C***H), 128.7 (PCH_2***C***), 121.7 (P***C***), 35.5 (Br***C***H_2), 32.7 (P***C***H_2), 7.77 (P***C***H_3). $^{31}P\{^1H\}$ NMR ($CDCl_3$): 24.3. ESI-MS (MeOH): *m/z* = 322.93 ($[M - Br]^+$). The synthesis was continued according to **GP2** whereby 2.2 g (5.3 mmol) of phosphonium bromide was used. HPLC fractions were collected at 16.4 min to afford the desired deprotected bifunctional ligand. Yield 1.91 g (51%). T_R = 16.4 min. $^1H\{^{31}P\}$ NMR (D_2O): δ = 7.85-7.65 (m, 5H, P-Ph***H***), 7.53 (d, 2H, $^3J_{HH}$ = 7.58, PCH_2CC***H***), 7.18 (d, 2H, $^3J_{HH}$ = 7.87 Hz, NCH_2CC***H***), 3.99 (s, 2H, PC***H***$_2$), 3.62-3.11 (m, 24H, C***H***$_2$), 2.24 (s, 6H, C***H***$_3$). $^{13}C\{^1H\}$ NMR (D_2O): δ = 134.7 (***C***$_{aryl}$), 131.6-131.2 (***C***$_{aryl}$), 130.3-129.7 (***C***$_{aryl}$), 122.1 (***C***$_{aryl}$), 119.2 (***C***$_{aryl}$), 118.3 (***C***H_2), 114.4 (***C***H_2), 110.5 (***C***H_2), 57.3-42.3 (***C***H_2), 5.6 (***C***H_3). $^{31}P\{^1H\}$ NMR (D_2O): δ = 23.7. ^{19}F (D_2O): δ = -75.51. ESI-FT-ICR-MS for $[M - CF_3CO_2]^+$: Calculated *m/z*

587.29930; Found 587.29930. Gd(III) complex **3** was synthesized according to **GP3** using 0.200 g (0.286 mmol) of the deprotected bifunctional ligand. HPLC fractions were collected at 16.2 min to afford the desired product. Yield 0.22 g (89%). T_R = 16.2 min. IR (KBr, cm^{-1}): $\tilde{\nu}$ = 1681 (C=O), TFA^-), 1594 (C=O), DO3A). M.p.>260°C (dec.). ESI-FTICR-MS for $[M - CF_3CO_2]^+$: Calculated *m/z* 742.20045; Found 742.20064.

Biological Assays

General: Two different cell lines were used for the biological studies. The tumor cell line employed was human glioblastoma multiforme (T98G), and the normal cell line used was human fetal glial cells (SVG p12). Both cell lines were purchased from ATCC and were grown as monolayers in Eagle's minimal essential medium (EMEM) supplemented with fetal bovine serum (FBS)(10% v/v), L-glutamine (2.5 mM), and an antibiotic anti-mycotic solution (AA) which contains penicillin (10,000 units/mL), streptomycin (10 mg/mL) and amphotericin B (25 mg/mL). Incubation for all biological studies was performed at 37°C in a humidified 5% CO_2 atmosphere. Cells were grown to >80% confluence before they were harvested with trypsin (0.1% *v/v*) from a 75-cm^2 flask and pelleted by means of centrifugation (2000 rpm for 3 min). Cell counting was performed on a Countess® Automated Cell Counter from Life Technologies.

Cytotoxicity Assays: Cytotoxicity assays were performed for complexes **1 – 3** using the 3-(4,5-dimethylthiazol-2-yl)-2,5-diphenyltetrazolium bromide (MTT) assay [30]. T98G cells were harvested with trypsin (0.1% *v/v*) from a 75-cm^3 flask and pelleted by means of centrifugation. The cells were re-suspended in complete EMEM and

counted using a hemocytometer (Weber). The cells were seeded with complete EMEM into a 96-well plate such that each well contained 100 μL and 1 × 10^4 cells. The plate was incubated overnight to allow the cells to adhere to the wells. The plate was then dosed with the selected Gd(III) complex by means of serial dilutions with a maximum concentration (C_{max}) of 4 mM (N = 4). Each plate included a vehicle control, V_C, (MQ water and EMEM), a positive control, C_{pos}, (cells and EMEM) and a negative control, C_{neg}, (Gd(III) complex and EMEM). The dosed plate was incubated for 72 h. The MTT solution in PBS (1.7 mg/mL) was added to each well (30 μL) and a further 4 h of incubation followed. The solution was removed from each well before DMSO (150 μL) was added to dissolve the MTT-formazan crystals. Cell viability was assessed by measuring the absorbance at 600 nm using a Victor3V microplate reader (PerkinElmer). Absorbance measurements were normalised to the C_{pos} wells such that the level of MTT was expressed as % cell viability according to these wells. A plot of log concentration *vs* % cell viability was generated by using GraphPad Prism® 6. IC_{50} values were determined as the concentration of complex required to cause a 50% decrease in cell viability.

Cell Uptake Studies: Three concentrations of complexes **1** – **3** (10 μM, 100 μM and 1000 μM) were assessed for their *in vitro* uptake by the T98G and SVG p12 cell lines. Three solutions of each Gd(III) complex were made up to the necessary concentrations using MQ water. Three individual repeats of each concentration as well as control experiments were conducted on each cell line.

T98G cells were cultured in 25-cm^3 flasks for 3 days to reach confluence. For the dosed flasks, the medium was replaced with dosed medium and then the flasks were incubated for a further 48 h. For the control flasks, the medium was replaced by fresh

medium with the appropriate volume of MQ water to afford a vehicle control and incubated for a further 48 h. Medium was then removed and the cells were washed with PBS to remove cell debris. The cells were harvested with trypsin (0.1% *v/v*) and then pelleted and re-suspended in PBS buffer (1 mL) twice. A 100 μL aliquot was taken out and set aside for protein analysis. Another 100 μL aliquot was isolated for cell counting. The remaining 0.8 mL cell suspension was centrifuged to afford a cell pellet which was analysed for Gd content by means of ICP-MS. The above procedure was repeated for the Gd uptake study using the SVG p12 cell line.

The cell pellets were digested in HNO_3 (0.5 mL, 69%) at 65°C in a water bath for 18 h. The digest was diluted to 10 mL with HCl (0.1 M), and then measured for Gd by means of ICP-MS. ICP-MS was run on a PerkinElmer ELAN 6100 Inductively Coupled Plasma Emission Mass Spectrometer (ICP-MS) at the Solid State and Elemental Analysis Unit (UNSW Analytical Centre). Metal uptake concentrations are reported in ng Gd/mg protein and Gd atoms/cell.

Protein Analysis: The protein content of cell solutions was determined using a bicinchoninic acid (BCA) protein assay, which has been described previously [40]. This assay involves the reduction of Cu(II) to Cu(I) by proteins and the subsequent chelation of Cu(I) by two molecules of BCA which results in a colour change that can be measured and compared to a protein standard curve. To perform the assay the cells were lysed by means of three snap freeze-thaw cycles which released the intracellular contents. The solution was analysed for protein content by taking repeated 25 μL samples (N = 3) and depositing them into a 96-well plate format. A 1 mg/mL bovine serum albumin (BSA) protein standard (200, 400, 800, and 1000 mg/mL, made up to volume with MQ water) was also deposited into the 96-well plate.

A freshly prepared solution of BCA and $CuSO_4 \cdot 5H_2O$ (50:1, 200 μL) was added to each well and the plate was incubated at 37 °C for 30 min. Absorbance was then measured at 600 nm using a victor3V microplate reader (PerkinElmer). The protein standard curve was fitted using linear regression which allowed for the determination of the protein content in unknown samples. Microsoft Office Excel® 2007 was used for all calculations and graphs.

Synchrotron X-ray Fluorescence (XRF) Imaging

Buffer Preparation: All buffers were freshly prepared on the day of the actual experiment. All solutions were filter-sterilized before use using a 0.22 μm syringe filter.

(a) Paraformaldehyde Solution: 1 g of powdered paraformaldehyde and 1 NaOH pellet were dissolved in 6 mL of PBS. The pH was adjusted to 7.2 with NaOH and HCl using a pH-meter. 1 mL of this freshly prepared solution was taken and diluted with 9 mL PBS to give a 1% paraformaldehyde solution.

(b) Piperazine-*N,N'*-bis(2-ethanesulfonic acid) (PIPES) / Sucrose Buffer: 50 mL buffer solution was prepared with milli-Q water and a final concentration of 20 mM PIPES and 200 mM sucrose, respectively. The pH was adjusted to 7.05 with acetic acid using a pH-meter.

(c) Sucrose Buffer: 50 mL buffer solution was prepared with milli-Q water and a final concentration of 250 mM sucrose. The pH was adjusted to 7.01 with acetic acid using a pH-meter.

Sample Preparation: The 500 nm thick Si_3N_4 windows (Silson Pty Ltd) were washed with 70% ethanol, PBS and EMEM. One window was placed in a well of a 12-well plate. T98G human glioblastoma cells were seeded directly on the Si_3N_4 windows with a density of 10^5 cells per well. The cells were allowed to adhere onto the Si_3N_4 windows overnight at 37 °C in a humidified 5% CO_2 atmosphere. The old medium was removed and the cells were incubated for 24 h in the presence of 100 μM of **1** or **2** (2 mL per well; solutions were filter-sterilized before use) in EMEM (treated cells) or for 24 h with EMEM alone (control cells).

Fixation Protocol: Following incubation the cell culture medium was gently removed and one Si_3N_4 window was placed in a new well of a 6-well plate. For the fixation of the cells the pre-heated 1% paraformaldehyde solution (37 °C in water bath) was added to the well just to cover the window (*ca.* 0.5 mL). After 20 min at RT the Si_3N_4 window was transferred to a new well and PIPES / sucrose buffer was added for 2 min just to cover the window. This last step was repeated twice; each time transferring the Si_3N_4 window to a new well (total of 3 washes with PIPES / sucrose buffer). Finally, the window was washed with sucrose buffer for 2 min (window just covered) twice; each time transferring the Si_3N_4 window to a new well. The Si_3N_4 windows were placed on a cellulose paper and allowed to dry on air for 1 h (cellulose paper placed between two well plates being covered with a well plate lid).

X-ray Fluorescence Imaging: The distribution of elements in cells was determined at the XFM beamline at the Australian Synchrotron [41]. An incident beam of 12.7 keV X-rays was used for the elemental mapping. The energy was chosen to induce *K*-shell ionization of Zn (naturally-high abundance at the cell nucleus) and *L*-shell ionization of Gd while also separating the scatter peaks from the fluorescence of

lighter elements. The incident beam was focused to a spot ~ 2 μm (full-width at half-maximum, fwhm) using a Kirkpatrick-Baez mirror pair. The specimen was continuously scanned through the focus using a step size of 2 μm, well-matched to the dimensions of the beam spot. Full XRF spectral images were obtained at each pixel with an effective dwell time of ~ 15 ms resulting in scans of ~100 cells collected in less than 2 h each. The low-latency, solid angle 384-channel Maia detector was positioned in the backscatter geometry. The resulting elemental maps ranged up to 400 000 pixels in size. During these experiments single element foils, Mn, Fe and Pt (Micromatter, Canada), were scanned in the same geometry and used as references to establish elemental quantitation. Deconvolution of the Maia data was performed using GeoPIXE v6.4w (CSIRO, Australia) that incorporates a linear transformation matrix to perform spectral deconvolution [42]. Spectra were calibrated using the metal foil measurements, and corrections made for self-absorption in the sample, absorption in air, and the efficiency response of the detector [43]. The detected X-ray photons from each pixel were related to calculated-model fluorescence X-ray yields for an assumed specimen composition and thickness. The composition and thickness of the Si_3N_4 window were known from the manufacturer, while the composition and average density typical of dried organic material ($C_{22}H_{10}N_2O_4$ and 1.42 g cm^{-3}, respectively) was used to model the bulk cell [44]. Absorption effects for XRF from the lowest atomic number element relevant to this study (Ca $K\alpha$ radiation for the Maia) are negligible for this specimen type.

Given the low energy resolution of the Maia detector, some potential exists for interference on the Gd $L\alpha$ signal from either Mn $K\alpha/\beta$ or Fe $K\alpha$, as well as other interferences on other Gd *L* lines from other elements. However, the Mn and Fe

concentrations in untreated cells were at or near the detection limit for the instrument with the parameters used, as assessed by noting minimal changes in signal between intracellular regions and background Si_3N_4 (i.e. cell outlines or other cellular features were not observed in either the Mn or Fe maps). An estimate of the background signal for Gd can be drawn from the control cell elemental contents presented in Table 2, which include possible contributions from Mn and Fe fluorescence. The Gd contents in treated cells were found to be at least two orders of magnitude greater than the background signal (except for the 10 μM SVG cells) and so it is assumed that the reported elemental maps and cellular contents in treated cells are not significantly interfered with by either the Mn or Fe signals.

Image Analysis: Image analysis of elemental maps was performed using a combination of tools native to *GeoPIXE* and *ImageJ* (v1.49j), a java-based image processing program developed by the National Institutes of Health (USA) [45].

Acknowledgments

We thank the Australian Research Council for funding, Dr Ian Luck (USyd) for assistance with NMR spectroscopy, and Dr Nick Proschogo (USyd) for assistance with the ESI-MS studies.

References

[1] P. Caravan, Chem. Soc. Rev. 35 (2006) 512-523.

[2] D. T. Schuehle, P. Caravan, in: J. Reedijk, K. Poeppelmeier (Eds.), Comprehensive Inorganic Chemistry II, 2nd ed., vol. 3, Metal-based MRI Contrast Agents, Elsevier, Oxford, 2013, pp. 901-932.

[3] S. Faulkner, O. A. Blackburn, in: N. J. Long, W.-T. Wong (Eds.), Chemistry of Molecular Imaging, The Chemistry of Lanthanide MRI Contrast Agents, John Wiley and Sons, Inc., Hoboken, New Jersey, 2015, pp. 179-197.

[4] A. Forouzannia, G. M. Richards, D. Khuntia, M. P. Metha, Expert Rev. Anticancer Ther. 7 (2007) 785-794.

[5] M. P. Metha, W. R. Shapiro, S. C. Phan, R. Gervais, C. Carrie, P. Chabot, R. A. Patchell, M. J. Glantz, L. Recht, C. Langer, R. K. Sur, W. H. Roa, M. A. Mahe, A. Fortin, C. Nieder, C. A. Meyers, J. A. Smith, R. A. Miller, M. F. Renschler, Int. J. Radiat. Oncol., Biol., Phys. 73 (2009) 1069-1076.

[6] T. D. Mody, J. L. Sessler, J. Porphyrins Phthalocyanines, 5 (2001) 134-142.

[7] G. De Stasio, D. Rajesh, J. M. Ford, M. J. Daniels, R. J. Erhardt, B. H. Frazer, T. Tyliszczak, M. K. Gilles, R. L. Conhaim, S. P. Howard, J. F. Fowler, F. Esteve, M. P. Mehta, Clin. Cancer Res., 12 (2006) 206-213.

[8] A. H. Soloway, W. Tjarks, B. A. Barnum, F.-G. Rong, R. F. Barth, I. M. Codogni, J. G. Wilson, Chem. Rev. 98 (1998) 1515-1562.

[9] E. L. Crossley, H. Y. V. Ching, J. A. Ioppolo, L. M. Rendina, In: E. Alessio (Ed.), Bioinorganic Medicinal Chemistry, Boron and Gadolinium in the Neutron Capture Therapy of Cancer, Wiley-VCH, Weinheim, Germany, 2011, pp. 283-305.

[10] E. L. Crossley, J. B. Aitken, S. Vogt, H. H. Harris, L. M. Rendina, Angew. Chem., Int. Ed., 49 (2010) 1231-1233.

[11] F. Issa, J. A. Ioppolo, L. M. Rendina, in: J. Reedijk, K. Poeppelmeier (Eds.), Comprehensive Inorganic Chemistry II, 2nd ed., Boron and Gadolinium Neutron Capture Therapy, Elsevier, Oxford, 2013, pp. 877-900.

[12] G. De Stasio, P. Casalbore, R. Pallini, B. Gilbert, F. Sanita, M. T. Ciotti, G. Rosi, A. Festinesi, L. M. Larocca, A. Rinelli, D. Perret, D. W. Mogk, P. Perfetti, M. P. Mehta, D. Mercanti, Cancer Res., 61 (2001) 4272-4277.

[13] B. H. Laster, W. C. Thomlinson, R. G. Fairchild, Radiat. Res. 133 (1993) 219-224.

[14] R. A. Miller, K. W. Woodburn, Q. Fan, I. Lee, D. Miles, G. Duran, B. Sikic, D. Magda, Clin. Cancer Res., 7 (2001) 3215-3221.

[15] W. N. William Jr., R. G. Zinner, D. D. Karp, Y. W. Oh, B. S. Glisson, S.-C. Phan, D. J. Stewart, J. Thorac. Oncol., 2 (2007) 745-750.

[16] T. Goorley, H. Nikjoo, Radiat. Res., 154 (2000) 556-563.

[17] D. E. Morrison, J. B. Aitken, M. D. de Jonge, F. Issa, H. H. Harris, L. M. Rendina, Chem. Eur. J., 20 (2014) 16602-16612.

[18] D. E. Morrison, J. B. Aitken, M. D. de Jonge, J. A. Ioppolo, H. H. Harris, L. M. Rendina, Chem. Commun. 50 (2014) 2252-2254.

[19] M. Busse; J. M. Fenton, L. M. Rendina, Aust. J. Chem., 68 (2015) 576-580.

[20] G. De Stasio, D. Rajesh, P. Casalbore, M. J. Daniels, R. J. Erhardt, B. H. Frazer, L. M. Wiese, K. L. Richter, B. R. Sonderegger, B. Gilbert, S. Schaub, R. J. Cannara, J. F. Crawford, M. K. Gilles, T. Tyliszczak, J. F. Fowler, L. M. Larocca, S. P. Howard, D. Mercanti, M. P. Mehta, R. Pallini, Neurol. Res., 27 (2005) 387-398.

[21] R. F. Martin, G. D'Cunha, M. Pardee, B. J. Allen, Pigm. Cell Res. 2 (1989) 330-332.

[22] R. F. Martin, G. D'Cunha, M. Pardee, B. J. Allen, Int. J. Radiat. Biol. 54 (1988) 205-208.

[23] D. C. Rideout, T. Calogeropoulou, J. S. Jaworski, R. Dagnino Jr., M. R. McCarthy, Anticancer Drug Des., 4 (1989) 265-280.

[24] J. S. Modica-Napolitano, J. R. Aprille, Cancer Res., 47 (1987) 4361-4365.

[25] S. Davis, M. J. Weiss, J. R. Wong, T. J. Lampidis, L. B. Chen, J. Biol. Chem., 260 (1985) 13844-13850.

[26] I. Madar, J. H. Anderson, Z. Szabo, U. Scheffel, P.-F. Kao, H. T. Ravert, R. F. Dannals, J. Nucl. Med., 40 (1999) 1180-1185.

[27] J. D. Steichen, M. J. Weiss, D. R. Elmaleh, R. L. Martuza, J. Neurosurg., 74 (1991) 116-122.

[28] A. N. Oksendal, P.A. Hals, J. Magn. Reson. Imaging, 3 (1993) 157-65.

[29] J. G. Penfield, R. F. Reilly Jr, Nat. Clin. Pract. Nephrol., 3 (2007) 654-68.

[30] T. Mosmann, J. Immunol. Methods, 65 (1983) 55-63.

[31] M. P. Mehta, W. R. Shapiro, M. J. Glantz, R. A. Patchell, M. A. Weitzner, C. A. Meyers, C. J. Schultz, W. H. Roa, M. Leibenhaut, J. Ford, W. Curran, S. Phan, J. A. Smith, R. A. Miller, M. F. Renschler, J. Clin. Oncol., 20 (2002) 3445-3453.

[32] P. Gros, F. Talbot, D. Tang-Wai, E. Bibi, H. R. Kaback, Biochemistry, 31 (1992) 1992-1998.

[33] P. K. Smith, R. I. Krohn, G. T. Hermanson, A. K. Mallia, F. H. Gartner, M. D. Provenzano, E. K. Fujimoto, N. M. Goeke, B. J. Olson, D. C. Klenk, Anal. Biochem. 150 (1985) 76-85.

[34] S. Aime, P. Caravan, J. Magn. Reson. Imaging, 30 (2009) 1259-1267.

[35] L. M. Plum, L. Rink, H. Haase, Int. J. Environ. Res. Public Health, 7 (2010) 1342-1365.

[36] R. A. Miller, K. Woodburn, Q. Fan, M. F. Renschler, J. L. Sessler, J. A. Koutcher, Int. J. Radiat. Oncol. Biol. Phys., 45 (1999) 981-989.

[37] W. L. F. Armarego, C. Chai, Purification of Laboratory Chemicals, 5th Ed., Elsevier, 2003.

[38] D. F. Shriver, The Manipulation of Air-Sensitive Compounds, McGraw-Hill, 1969.

[39] D. A. Moore, Org. Synth., 85 (2008) 10-14.

[40] P. K. Smith, R. I. Krohn, G. T. Hermanson, A. K. Mallia, F. H. Gartner, M. D. Provenzano, E. K. Fujimoto, N. M. Goeke, B. J. Olson, D. C. Klenk, Anal. Biochem., 150 (1985) 76-85.

[41] D. Paterson, M. D. de Jonge, D. L. Howard, W. Lewis, J. McKinlay, A. Starritt, M. Kusel, C. G. Ryan, R. Kirkham, G. Moorhead, AIP Conf. Proc. 1365 (2011) 219-222.

[42] C. G. Ryan, Int. J. Imaging Syst. Technol., 11 (2000) 219-230.

[43] C. G. Ryan, Nucl. Instrum. Methods Phys. Res., Sect. B, 181 (2001) 170-179.

[44] W. H. McMaster, N. Kerr del Grande, J. H. Mallett, J. H. Hubbell, National Technical Information Services L-3, U.S. Department of Commerce, Washington, D.C., 1969.

[45] C. A. Schneider, W. S. Rasband, K. W. Eliceiri, Nat. Methods, 9 (2012) 671-675.

Table 1: IC_{50} values (with standard errors) for complexes **1 – 3** in the T98G cell line ($N = 4$).

Complex	IC_{50} (mM)
1	2.55 ± 0.33
2	1.23 ± 0.06
3	2.76 ± 0.13

Table 2: ICP-MS analysis of Gd content (with standard errors) in T98G and SVG p12 cells treated with **1 – 3** for 48 h ($N = 3$).

Gd(III) complex	Gd(III) complex concentration (μM)	T98G cells		SVG p12 cells		T/N cell ratio	
		ng Gd/mg protein	Gd atoms/cell	ng Gd/mg protein	Gd atoms/cell	ng Gd/mg protein	Gd atoms/cell
Control	0	6.0 ± 2.2	$7.6 \times 10^6 \pm 4.1 \times 10^6$	9.1 ± 2.0	$1.1 \times 10^7 \pm 3.7 \times 10^6$	0.7 ± 0.1	0.2 ± 0.1
1	10	420.1 ± 5.4	$5.8 \times 10^8 \pm 6.8 \times 10^6$	31.8 ± 5.0	$3.8 \times 10^7 \pm 6.3 \times 10^6$	13.2 ± 2.1	15.2 ± 2.5
	100	1487.0 ± 146.1	$1.9 \times 10^9 \pm 2.8 \times 10^8$	308.7 ± 18.4	$4.2 \times 10^8 \pm 1.7 \times 10^7$	4.8 ± 0.6	4.5 ± 0.7
	1000	3000.3 ± 457.7	$4.0 \times 10^9 \pm 6.3 \times 10^8$	6440.5 ± 177.5	$8.4 \times 10^9 \pm 3.4 \times 10^8$	0.5 ± 0.1	0.5 ± 0.1
2	10	713.3 ± 44.1	$8.9 \times 10^8 \pm 5.3 \times 10^7$	133.7 ± 89.2	$2.6 \times 10^8 \pm 1.9 \times 10^8$	5.3 ± 3.6	3.4 ± 1.4
	100	7709.9 ± 1807.8	$1.0 \times 10^{10} \pm 2.4 \times 10^9$	1702.9 ± 387.6	$2.4 \times 10^9 \pm 5.3 \times 10^8$	4.5 ± 1.5	4.2 ± 0.5
	1000	28681.8 ± 2780.8	$3.7 \times 10^{10} \pm 3.7 \times 10^9$	13828.6 ± 3427.0	$1.8 \times 10^{10} \pm 4.5 \times 10^9$	2.1 ± 0.4	2.1 ± 0.4
3	10	201.0 ± 65.1	$3.9 \times 10^8 \pm 7.4 \times 10^7$	61.8 ± 17.4	$7.0 \times 10^7 \pm 1.6 \times 10^7$	3.3 ± 0.6	5.6 ± 0.6
	100	3462.0 ± 400.8	$4.9 \times 10^9 \pm 5.5 \times 10^8$	1068.0 ± 86.5	$1.3 \times 10^9 \pm 1.8 \times 10^8$	3.2 ± 0.2	3.8 ± 0.3
	1000	13986.7 ± 407.8	$1.8 \times 10^{10} \pm 5.6 \times 10^8$	11763.2 ± 836.7	$1.7 \times 10^{10} \pm 9.4 \times 10^8$	1.2 ± 0.1	1.1 ± 0.07

Captions to Figures and Schemes

Figure 1: Mean Gd uptake by individual T98G human glioblastoma cells (black bar) and SVG p12 human glial cells (grey bar) following treatment with Gd complexes **1 – 3** for 48 h at concentrations of 10 μM, 100 μM and 1000 μM in comparison to the control (i.e. cells not incubated with a Gd(III) complex) ($N = 3$), as determined by ICP-MS. Results were expressed as the mean ± SEM (ng Gd / mg protein). Ordinary two-way ANOVA (column factor: cell lines and row factor: treatment) followed by Sidak's multiple comparisons test ($P < 0.0001$ = ****) was performed using GraphPad Prism version 6.00 for Windows (www.graphpad.com).

Figure 2: Mean Gd uptake by individual T98G human glioblastoma cells and SVG p12 human glial cells following treatment with Gd(III) complexes **1 – 3** (grey, dark grey and light gray bar, respectively) for 48 h at concentrations of 10 μM, 100 μM and 1000 μM in comparison to the control (black bar; cells not incubated with a Gd(III) complex) ($N = 3$), as determined by ICP-MS. Results were expressed as the mean ± SEM (ng Gd / mg protein). Ordinary two-way ANOVA (column factor: Gd(III) complex and row factor: treatment) followed by Sidak's multiple comparisons test ($P > 0.05$ = ns; $P \leq 0.05$ = *; $P \leq 0.01$ = **; $P \leq 0.001$ = ***; $P < 0.0001$ = ****) was performed using GraphPad Prism version 6.00 for Windows (www.graphpad.com).

Figure 3: Tumor cell selectivity expressed as a ratio of Gd content in T98G and SVG p12 cells treated with **1 – 3** (black, grey and dark grey bars, respectively) for 48 h at concentrations of 10 μM, 100 μM and 1000 μM in comparison to the control (i.e. cells not incubated with a Gd(III) complex) ($N = 3$), as determined by ICP-MS. Results were derived from ng Gd / mg protein and expressed as mean ± SEM. Ordinary two-way ANOVA (column factor: treatment and row factor: concentration) followed by Sidak's multiple comparisons ($P < 0.0001$ = ****) test was performed using GraphPad Prism version 6.00 for Windows (www.graphpad.com).

Figure 4: Quantification of the cellular Gd load in a population of T98G cells. Elemental distribution maps of a representative area (~20% of total scan area) showing T98G cells either untreated or treated with 100 μM of complex **2** incubated for 6 h (**2** – 6 h) or 24 h (**2** – 24 h). Scale bar = 125 μm. Inelastic scatter (Compton) of incident photons was a useful guide to identify the cell boundaries. The color scheme for each element is scaled separately.

Figure 5: *First row of panels:* Inelastic scatter (Compton) map of incident photons showing the ROI (red square). The subsequent panels show the mask (yellow) derived from the Compton map (showing the magnified view of T98G cells), an overlay of the mask applied to high definition elemental maps to identify cells from non-cellular debris (based on the endogenous Zn content present

within cells) and the final panel shows the distribution of complex **2** within T98G cells (based on the distribution of Gd) relative to the position of cells. Scale bar = 125 μm. *Second row of panels:* High definition Zn map of treated T98G cells showing the ROI (red square). The subsequent panels show the mask (yellow) derived from the Zn map (showing the magnified view of T98G cells), an overlay of the mask applied to high definition elemental maps to identify cells from non-cellular debris (based on the endogenous Zn content present within cells) and the final panel shows the distribution of complex **2** within T98G cells (based on the distribution of Gd) relative to the position of cells. Scale bar = 125 μm. (**A**) T98G cells were treated with 100 μM of **2** incubated for 6 h and (**B**) T98G cells were treated with 100 μM of complex **2** incubated for 24 h.

Scheme 1: Synthesis of Gd(III) complexes containing an arylphosphonium centre. TFA = trifluoroacetic acid, DO3A-^{t}Bu$_3$·HBr = 1,4,7,10-tetraazacyclododecane-1,4,7-triacetic acid tri-*tert*-butyl ester hydrobromide, MeCN = acetonitrile.

Figure 1

Gd(III) complex concentration	10 μM	100 μM	1000 μM
Cell uptake	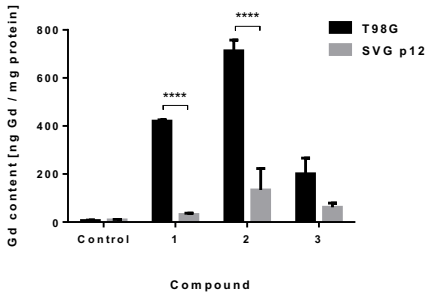	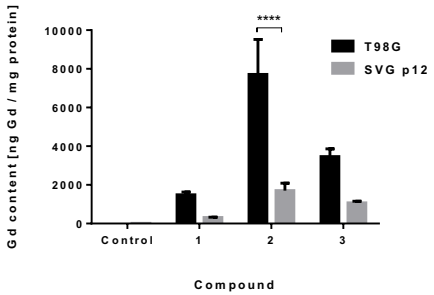	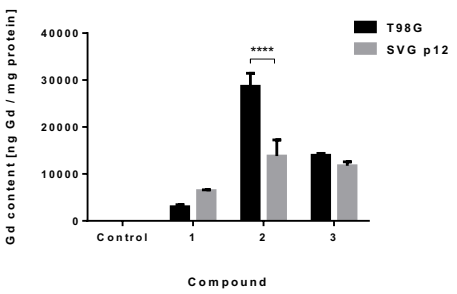

Figure 2

Gd(III) complex concentration	10 μM	100 μM	1000 μM
Cell uptake	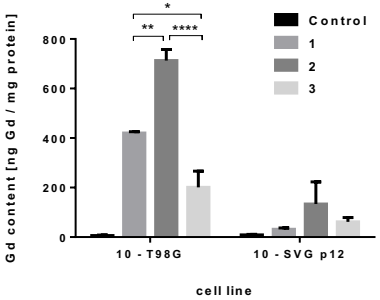	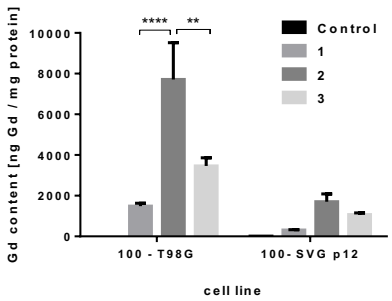	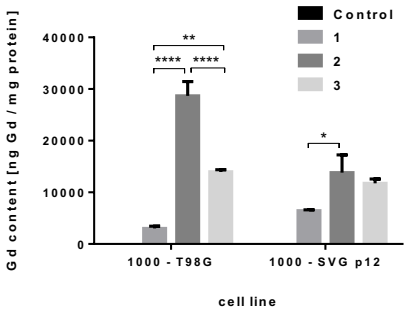

Figure 3

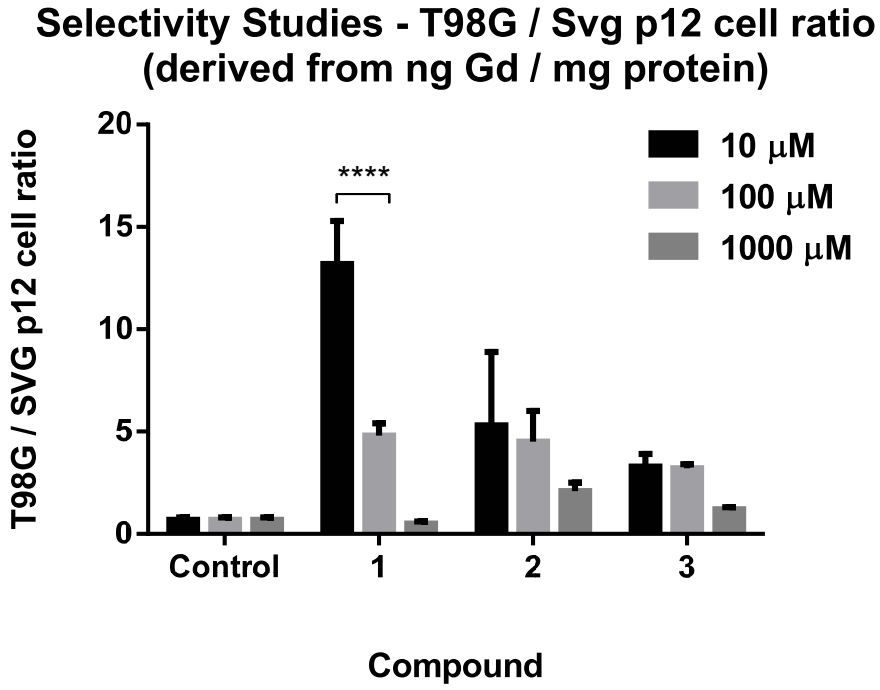
Selectivity Studies - T98G / Svg p12 cell ratio
(derived from ng Gd / mg protein)
T98G / SVG p12 cell ratio
20
15
10
5
0
****
10 μM
100 μM
1000 μM
Control
1
2
3
Compound

Figure 4

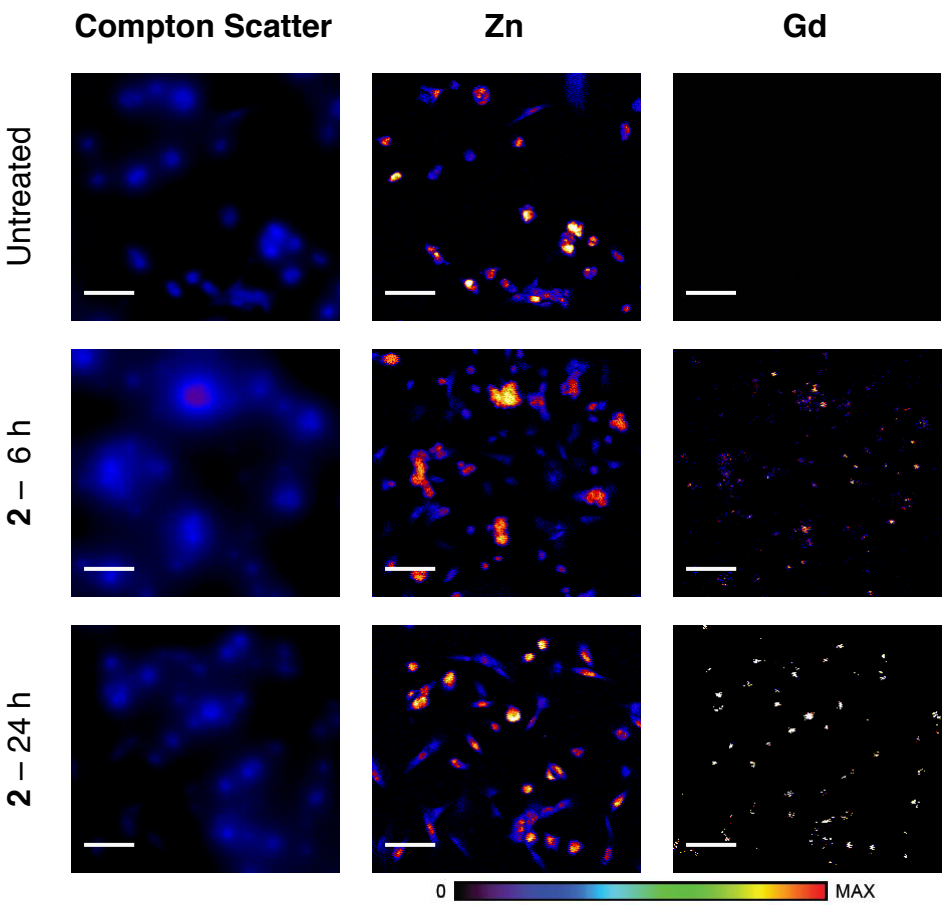

Figure 5

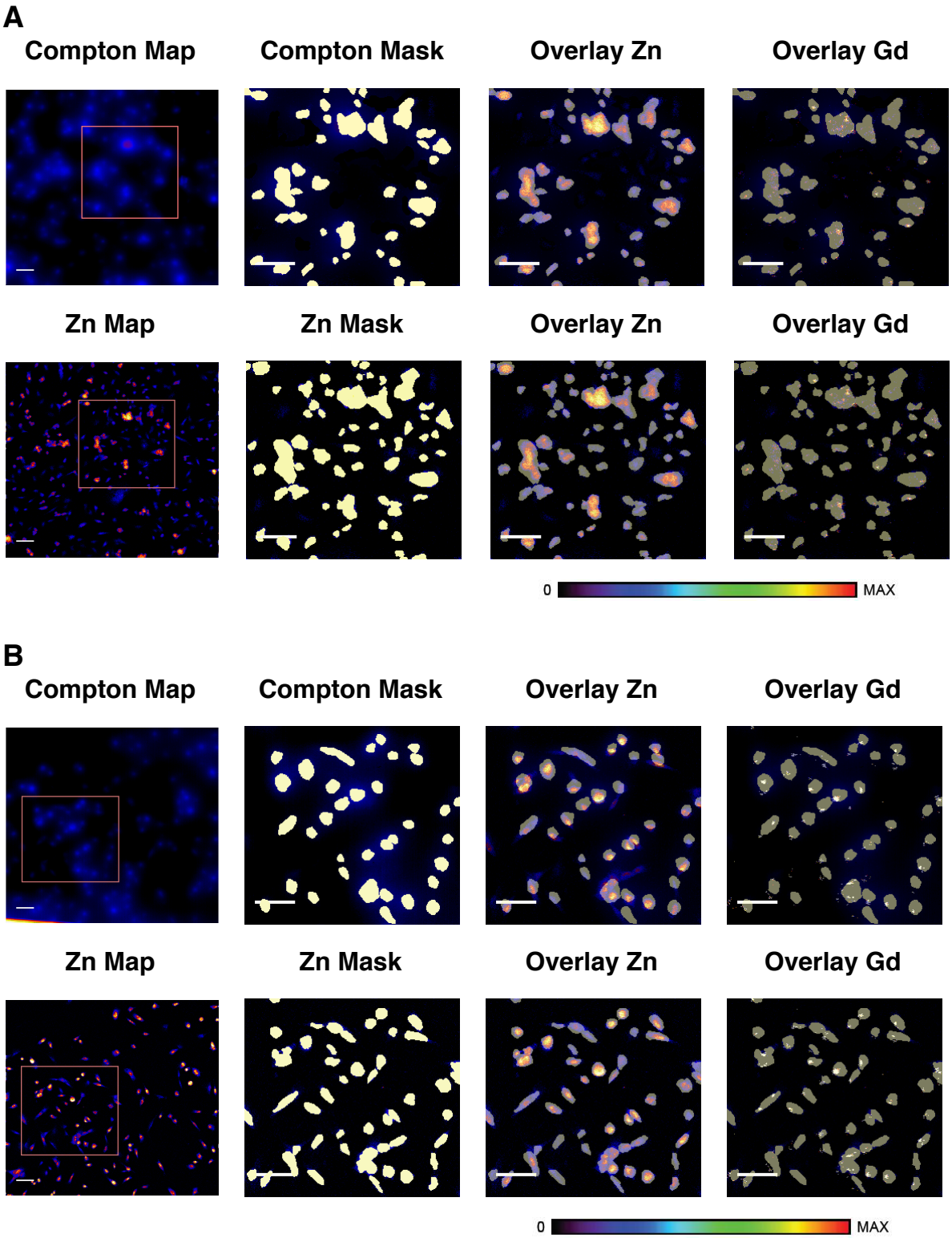
A
Compton Map
Compton Mask
Overlay Zn
Overlay Gd
Zn Map
Zn Mask
Overlay Zn
Overlay Gd
0
MAX
B
Compton Map
Compton Mask
Overlay Zn
Overlay Gd
Zn Map
Zn Mask
Overlay Zn
Overlay Gd
0
MAX

Scheme 1

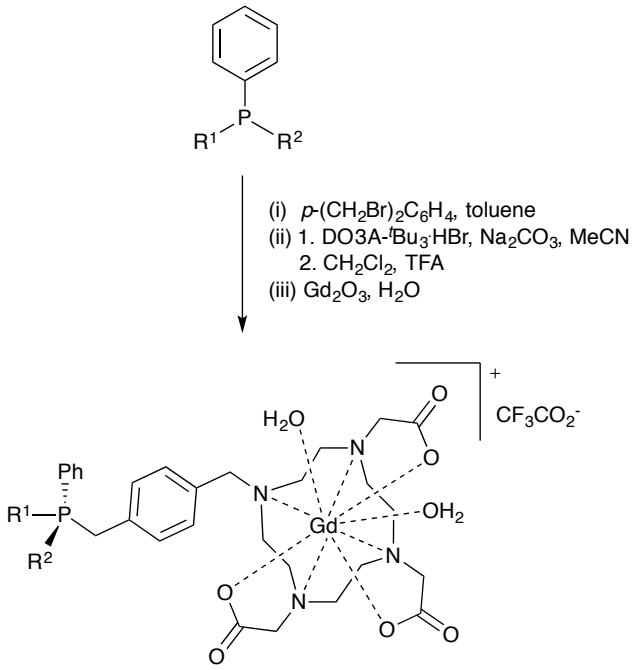

1: $R^1 = R^2 = Ph$
2: $R^1 = Ph$, $R^2 = Me$
3: $R^1 = R^2 = Me$